

Single-Sweep Methods for Free Energy Calculations

Luca Maragliano* and Eric Vanden-Eijnden†

Courant Institute of Mathematical Sciences, New York University, New York, NY 10012, USA

A simple, efficient, and accurate method is proposed to map multi-dimensional free energy landscapes. The method combines the temperature-accelerated molecular dynamics (TAMD) proposed in [Maragliano & Vanden-Eijnden, Chem. Phys. Lett. **426**, 168 (2006)] with a variational reconstruction method using radial-basis functions for the representation of the free energy. TAMD is used to rapidly sweep through the important regions of the free energy landscape and compute the gradient of the free energy locally at points in these regions. The variational method is then used to reconstruct the free energy globally from the mean force at these points. The algorithmic aspects of the single-sweep method are explained in detail, and the method is tested on simple examples, compared to metadynamics, and finally used to compute the free energy of the solvated alanine dipeptide in two and four dihedral angles.

I. INTRODUCTION

The free energy (or potential of mean force) is the thermodynamic force driving structural processes such as conformational changes of macromolecules in aqueous solution, ligand binding at the active site of an enzyme, protein-protein association, etc. The free energy gives information about both the rate at which these processes occur and the mechanism by which they occur. This makes free energy calculations a central issue in biophysics. Molecular dynamics (MD) simulations provide a tool for performing such calculations on a computer in a way which is potentially both precise and inexpensive (e.g. [1, 2, 3]). Since a free energy is in essence the logarithm of a probability density function (see (1) below for a precise definition) it can in principle be calculated by histogram methods based on the binning of an MD trajectory. This direct approach, however, turns out to be unpractical in general because the time scale required for the trajectory to explore all the relevant regions of configuration space is prohibitively long. Probably the best known and most widely used technique to get around this difficulty is the weighted histogram analysis method (WHAM) [4]. Following [5], WHAM adds artificial biasing potentials to maintain the MD system in certain umbrella sampling windows. WHAM then recombines in an optimal way the histograms from all the biased simulations to compute the free energy. WHAM is much more efficient than the direct sampling approach, and generalizations such as [6] alleviate somewhat the problem of where to put the umbrella windows (usually, this requires some *a priori* knowledge of the free energy landscape). In practice, however, WHAM remains computationally demanding and it only works to compute the free energy in 2 or 3 variables. An interesting alternative to WHAM is metadynamics [7, 8]. In essence metadynamics is a way to use an MD trajectory to place inverted umbrella sam-

pling windows on-the-fly and use these windows both to bias the MD simulation and as histogram bins to sample the free energy directly (thereby bypassing the need of further histogram analysis in each window).

Both WHAM and metadynamics compute the free energy directly by histogram methods, but an alternative approach is possible. Unlike the free energy which is a global quantity, its negative gradient (known as the mean force) can be expressed in terms of a local expectation and thereby computed at a given point in the free energy landscape. This is the essence of the blue moon sampling strategy [9] and it offers the possibility to calculate first the mean force at a given set of locations, then use this information to reconstruct the free energy globally. In one dimension, this approach is known as thermodynamic integration and it goes back to Kirkwood [10]. In higher dimensions, however, this way to compute free energies has been impeded by two issues. The first is where to place the points at which to compute the mean force, and the second is how to reconstruct the free energy from these data

In this paper, we propose a method, termed single-sweep method, which addresses both of these issues in two complementary but independent steps. In a first step, we use the temperature-accelerated molecular dynamics (TAMD) proposed in [11] (see also [12, 13]) to quickly sweep through the important regions of the free energy landscape and identify points in these regions where to compute the mean force. In the second step we then reconstruct the free energy globally from the mean force by representing the free energy using radial-basis functions, and adjusting the parameters in this representation via minimization of an objective function.

The single-sweep method is easy to use and implement, does not require *a priori* knowledge of the free energy landscape, and can be applied to map free energies in several variables (up to four, as demonstrated here, and probably more). The single-sweep method is also very efficient, especially since the mean force calculations can be performed using independent calculations on distributed processors (i.e. using grid computing facilities [14, 15]).

The remainder of this paper is organized as follows. In Sec. II, we describe the two steps of the single-sweep

*Electronic address: maraglia@cims.nyu.edu

†Electronic address: eve2@cims.nyu.edu

method in detail, starting with the second one for convenience. In Sec. III we illustrate the method on a simple two-dimensional example. This example is then used for comparison with metadynamics in Sec. IV. In Sec. V we use the single-sweep method to compute the free energy of alanine dipeptide (AD) in solution in two and in four of its dihedral angles. Finally, concluding remarks are made in Sec. VI and the details of the MD calculation on AD are given in Appendix A

II. THE SINGLE-SWEEP METHOD

A. Free energy representation and reconstruction

We shall consider a molecular system with n degrees of freedom whose position in configuration space $\Omega \subseteq \mathbb{R}^n$ will be denoted by \mathbf{x} . We also introduce a set of N collective variables $\boldsymbol{\theta}(\mathbf{x}) = (\theta_1(\mathbf{x}), \dots, \theta_N(\mathbf{x}))$ which are functions of \mathbf{x} such as torsion angles, interatomic distances, etc. If $V(\mathbf{x})$ denotes the potential energy of the system and $1/\beta$ its temperature, the free energy $A(\mathbf{z})$ in the variables $\boldsymbol{\theta}(\mathbf{x})$ is defined as

$$A(\mathbf{z}) = -\beta^{-1} \log \int_{\Omega} e^{-\beta V(\mathbf{x})} \delta(\boldsymbol{\theta}(\mathbf{x}) - \mathbf{z}) d\mathbf{x} \quad (1)$$

so that $e^{-\beta A(\mathbf{z})}$ is, up to a proportionality constant, the probability density function (PDF) of the variables $\boldsymbol{\theta}(\mathbf{x})$.

As mentioned in the introduction, the negative gradient of the free energy, $\mathbf{f}(\mathbf{z}) = -\nabla_{\mathbf{z}} A(\mathbf{z})$, is known as the mean force, and it can be computed locally at point \mathbf{z} via calculation of an expectation (see (11) below). In this section, we shall suppose that we have obtained an estimate of $\mathbf{f}(\mathbf{z})$ at points $\mathbf{z}_1, \dots, \mathbf{z}_K$, and we focus on the reconstruction of the free energy $A(\mathbf{z})$ from these data. A specific way to pick these points and compute $\mathbf{f}_1 \approx \mathbf{f}(\mathbf{z}_1), \dots, \mathbf{f}_K \approx \mathbf{f}(\mathbf{z}_K)$ will be given in Sec. II B, but it is worth pointing out that the reconstruction method proposed here works with data set collected in any other ways.

Our reconstruction method uses a radial-basis function representation for the free energy $A(\mathbf{z})$ with centers at $\mathbf{z}_1, \dots, \mathbf{z}_K$ [16, 17]:

$$\tilde{A}(\mathbf{z}) = \sum_{k=1}^K a_k \varphi_{\sigma}(|\mathbf{z} - \mathbf{z}_k|) + C. \quad (2)$$

Here C is a constant used to adjust the overall height of $\tilde{A}(\mathbf{z})$ but is otherwise irrelevant, $|\cdot|$ denotes the Euclidean norm in \mathbb{R}^N , and $\varphi_{\sigma}(u) = \varphi(u/\sigma)$ where $\varphi(u)$ is a radial-basis function; a convenient choice is to use the Gaussian packet

$$\varphi(u) = e^{-\frac{1}{2}u^2} \quad (3)$$

though other radial-basis functions (multiquadric, Sobolev splines, Wendland, etc. [16]) can be used as well,

see Sec. V. In (2) the heights a_k and the radial-basis function width $\sigma > 0$ are adjustable parameters which we determine by minimizing over a_k and σ the following objective function, which measures the discrepancy between the negative gradient of the function $\tilde{A}(\mathbf{z})$ in (2) at the centers \mathbf{z}_k , $\nabla_{\mathbf{z}} \tilde{A}(\mathbf{z}_k) = \sum_{k'=1}^K a_{k'} \nabla_{\mathbf{z}} \varphi_{\sigma}(|\mathbf{z}_k - \mathbf{z}_{k'}|)$, and the mean force \mathbf{f}_k estimated at these centers:

$$E(a, \sigma) = \sum_{k=1}^K \left| \sum_{k'=1}^K a_{k'} \nabla_{\mathbf{z}} \varphi_{\sigma}(|\mathbf{z}_k - \mathbf{z}_{k'}|) + \mathbf{f}_k \right|^2. \quad (4)$$

Before explaining how we perform this minimization, let us give several reasons why the radial-basis representation (2) for $A(\mathbf{z})$ is natural and convenient. First, the centers \mathbf{z}_k in (2) do not have to lie on a regular grid, which permits to use mean force data collected anywhere. Second, the representation (2) can be used in any dimension. Third, this representation has very good convergence properties, i.e. a small number of centers gives an accurate representation of $A(\mathbf{z})$. In fact, unlike standard representations based e.g. on linear interpolation on a regular grid, the rate of convergence in K of the representation in (2) can be made independent of N (a feature which the radial-basis representations share with sparse grids [18, 19]).

Going back to the minimization of $E(a, \sigma)$, it can be performed as follows. For fixed σ , the a_k^* minimizing (4) solve the following linear algebraic system

$$\sum_{k'=1}^K B_{k,k'}(\sigma) a_{k'}^*(\sigma) = c_k(\sigma) \quad (5)$$

where $B_{k,k'}(\sigma)$ and $c_k(\sigma)$ are given by

$$\begin{aligned} B_{k,k'}(\sigma) &= \sum_{k''=1}^K \nabla_{\mathbf{z}} \varphi_{\sigma}(|\mathbf{z}_k - \mathbf{z}_{k''}|) \cdot \nabla_{\mathbf{z}} \varphi_{\sigma}(|\mathbf{z}_{k''} - \mathbf{z}_{k'}|), \\ c_k(\sigma) &= - \sum_{k'=1}^K \nabla_{\mathbf{z}} \varphi_{\sigma}(|\mathbf{z}_k - \mathbf{z}_{k'}|) \cdot \mathbf{f}_{k'}. \end{aligned} \quad (6)$$

Given the centers \mathbf{z}_k and the estimates \mathbf{f}_k of the mean force at these centers, the coefficients $B_{k,k'}$ and c_k can be easily computed, and the linear system (5) can be solved by any standard technique, e.g. Gaussian elimination. Once the solution $a_k^* \equiv a_k^*(\sigma)$ of (5) is determined, to find the optimal σ^* satisfying $E(a^*(\sigma^*), \sigma^*) = \min_{\sigma} E(a^*(\sigma), \sigma)$ we compute the residual $E(a^*(\sigma), \sigma)$ for increasing values of σ starting from the distance between the centers. More sophisticated procedures could be used to minimize $E(a^*(\sigma), \sigma)$ over σ , but the brute force method that we used proved to be efficient enough because computing successive solutions of (5) for various σ is very fast. To measure the error in the approximation, we used the residual per center defined as

$$e_2(\sigma) = E^{1/2}(a^*(\sigma), \sigma) / K, \quad (7)$$

which reaches its minimum value at the same σ^* as $E(a^*(\sigma), \sigma)$.

Overall, the procedure is simple and inexpensive since the determination of a_k^* at fixed σ is computationally straightforward and cheap, and can be easily repeated to perform the one-dimensional minimization over σ . One caveat that we should mention, however, is that the condition number of the matrix $B_{k,k'}(\sigma)$ increases rapidly when the number of centers and/or σ increase. This is a known problem of radial-basis functions [17]. To avoid any problems, we capped the admissible condition number at 10^{12} and, in situations where this threshold value was reached while $e_2(\sigma)$ was still decreasing, picked for σ^* the corresponding value of σ . These situations only occurred in the two-dimensional example (see Sec. III) when a lot of centers were used (500 or more, i.e. much more than what will be used in the AD example), and even in these cases, such a large condition number did not lead to any noticeable loss of accuracy in the results (even though the coefficients a_k^* were then very large). We also observed that, given a number of centers \mathbf{z}_k and a value of σ , the condition number is typically lower when the dimension of \mathbf{z} is larger. Finally, we observed that the condition number was much lower with the Wendland radial-basis function (see (16) in Sec. V) than with the Gaussian radial-basis function (3).

B. TAMM for sweeping

It remains to explain how to identify the centers $\mathbf{z}_1, \dots, \mathbf{z}_K$ and estimate the mean force at these points. Following [11], we will do so using the extended system

$$\begin{cases} M\ddot{\mathbf{x}} = -\nabla_x V(\mathbf{x}) - \kappa \sum_{\alpha=1}^N (\theta_\alpha(\mathbf{x}) - z_\alpha) \nabla_x \theta_\alpha(\mathbf{x}) \\ \quad + \text{thermostat terms at } \beta^{-1} \\ \gamma \dot{\mathbf{z}} = \kappa(\boldsymbol{\theta}(\mathbf{x}) - \mathbf{z}) + \sqrt{2\gamma\bar{\beta}^{-1}} \boldsymbol{\eta}(t) \end{cases} \quad (8)$$

where M is the mass matrix, $\boldsymbol{\eta}(t)$ is a white-noise, i.e. a Gaussian process with mean 0 and covariance $\langle \eta_\alpha(t) \eta_{\alpha'}(t') \rangle = \delta_{\alpha\alpha'} \delta(t-t')$, and $\kappa > 0$, the friction coefficient $\gamma > 0$ and the artificial inverse temperature $1/\bar{\beta} (\neq 1/\beta)$ are parameters whose role we explain now.

The system in (8) describes the motion of \mathbf{x} and \mathbf{z} over the extended potential

$$U_\kappa(\mathbf{x}, \mathbf{z}) = V(\mathbf{x}) + \frac{1}{2} \kappa |\boldsymbol{\theta}(\mathbf{x}) - \mathbf{z}|^2. \quad (9)$$

As shown in [11], by adjusting the parameter κ so that $\mathbf{z}(t) \approx \boldsymbol{\theta}(\mathbf{x}(t))$ and the friction coefficient γ so that \mathbf{z} moves slower than \mathbf{x} , one can generate a trajectory $\mathbf{z}(t)$ in \mathbf{z} -space which effectively moves at the artificial temperature $1/\bar{\beta}$ on the free energy computed at the physical temperature $1/\beta$. By taking $1/\bar{\beta} > 1/\beta$, the $\mathbf{z}(t)$ trajectory visits rapidly the regions where the free energy is relatively low (i.e. within a range of a few $1/\bar{\beta}$) even if these regions are separated by barriers which the system

would take a long time to cross at the physical temperature $1/\beta$. This gives us a way to determine automatically where are the relevant regions in free energy space.

In [11], the extended system in (8) was proposed to sample the free energy landscape directly. Here, we make a different use of (8): we utilize the trajectory $\mathbf{z}(t)$ to rapidly sweep through \mathbf{z} -space and generate the centers $\mathbf{z}_1, \dots, \mathbf{z}_K$ used in the radial-basis representation (2). Specifically, we start from $\mathbf{z}(0) = \mathbf{z}_1$, then deposit a new center \mathbf{z}_k along $\mathbf{z}(t)$ each time $\mathbf{z}(t)$ reaches a point which is more than a prescribed distance d away from all the previous centers, where d is a parameter controlling the density of the covering by the centers (the smaller d , the higher the number of centers deposited). At the same time, at each of these centers \mathbf{z}_k , we launch a simulation of (8) with $\mathbf{z}(t) = \mathbf{z}_k$ fixed, i.e we use

$$M\ddot{\mathbf{x}} = -\nabla_x V(\mathbf{x}) - \bar{\kappa} \sum_{\alpha=1}^N (\theta_\alpha(\mathbf{x}) - z_{k,\alpha}) \nabla_x \theta_\alpha(\mathbf{x}) \quad (10) \\ + \text{thermostat terms at } \beta^{-1}$$

and compute:

$$\mathbf{f}_k = \frac{1}{T} \int_0^T \bar{\kappa} (\mathbf{z}_k - \boldsymbol{\theta}(\mathbf{x}(t))) dt. \quad (11)$$

The calculations of these time averages are independent of each other, and hence they can be distributed, using (ideally) at least one processor per center \mathbf{z}_k , an approach that optimally fits with the purposes of grid computing [14, 15]. The estimator in (11) has the advantage of being simple, but it introduces an error due to the finiteness of $\bar{\kappa}$. This error can be decreased by using $\bar{\kappa}$ in (10) and (11) larger than κ in (8), or even eliminated by using constrained instead of restrained simulations and using the blue-moon estimator for the mean force [20, 21].

Once the centers $\mathbf{z}_1, \dots, \mathbf{z}_K$ have been deposited and the estimates $\mathbf{f}_1, \dots, \mathbf{f}_K$ of the mean force at these centers have been obtained, we use the reconstruction procedure explained in Sec.IIA and compute the optimal set of coefficients a_k^* and the optimal σ^* to use in the representation (2) for $A(\mathbf{z})$.

We conclude this section by stressing that using the extended dynamics (8) to sweep through \mathbf{z} -space and deposit the centers \mathbf{z}_k is very different than using it to sample $A(\mathbf{z})$ directly, which makes our approach very different from WHAM or metadynamics. Unlike with sampling, revisiting twice a region in \mathbf{z} -space is unnecessary and even undesirable since no new center will be deposited. The accuracy of the reconstruction depends on the number of centers and the accuracy at which the mean force is computed in (11) much more than the precise locations where the centers are deposited. An important practical consequence is that it is rather straightforward to pick the parameters κ and γ in (8) since the final result is robust against variations in these parameters.

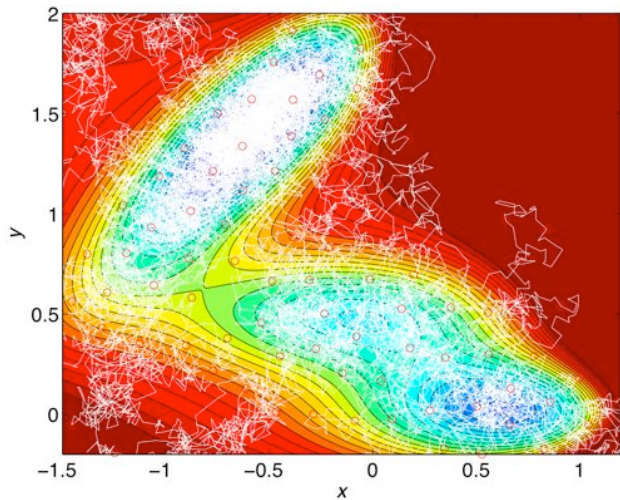


FIG. 1: A trajectory generated by simulating (12) by forward Euler with a time-step $\Delta t = 2 \cdot 10^{-5}$ for $2 \cdot 10^4$ steps (white curve) shown above the contour plot of the Mueller potential (with 29 level sets evenly distributed between $V = 0$ and $V = 180$ in a scale where the minimum of the potential is $V = 0$). The red circles are the locations of the centers deposited along the trajectory using $d = 0.175$. In this run, 174 centers were deposited.

III. TWO-DIMENSIONAL ILLUSTRATIVE EXAMPLE

Since, given the location of the centers \mathbf{z}_k , the mean force estimation at these points is quite standard, as a first illustration we use a two-dimensional example for which $\boldsymbol{\theta}(\mathbf{x}) \equiv \mathbf{x} = (x, y)$ and $A(\mathbf{z}) \equiv V(\mathbf{x})$ where $V(\mathbf{x})$ is the Mueller potential [22]. In this case, there is no need to extend the system as in (8), and the temperature accelerated dynamics simply reduces to (setting $\gamma = 1$ by appropriate rescaling of time)

$$\dot{\mathbf{x}} = -\nabla V(\mathbf{x}) + \sqrt{2\beta^{-1}} \boldsymbol{\eta}(t). \quad (12)$$

Fig. 1 shows a TAMD trajectory generated by solving (12) by forward Euler with the initial condition $(x(0), y(0)) = (1, 0)$ and a time-step of $\Delta t = 2 \cdot 10^{-5}$ for $2 \cdot 10^4$ time-steps at $1/\beta = 40$ (for comparison the energy barrier between the two main minima of the Mueller potential is about 100). Also shown are the centers $\mathbf{z}_k \equiv (x_k, y_k)$ obtained by depositing a new center along the trajectory each time the trajectory reaches a point which is $d = 0.175$ away for all the previous centers. In this run, 174 centers were deposited. At the centers, we used $-\nabla V(x_k, y_k) = \mathbf{f}_k$ as estimate of the “mean force” (i.e. there is no sampling error in the present example). We then used these data to reconstruct the free energy as explained in Sec. II A. Fig. 2 shows the residual per center $e_2(\sigma)$ defined in (7). The optimal σ for this run was $\sigma^* = 0.398$ and the condition number at this σ^* was $7 \cdot 10^6$. The level sets of the reconstructed potential are shown in Fig. 3 and compared to those of the

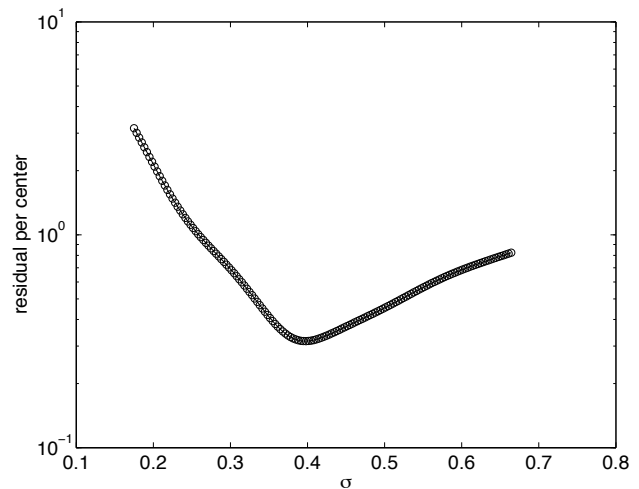


FIG. 2: Residual per center $e_2(\sigma)$ defined in (7) for the reconstruction of the Mueller potential with the $2 \cdot 10^4$ steps single-sweep trajectory shown in Fig. 1. The optimal σ for this run was $\sigma^* = 0.398$.

original Mueller potential, while Fig. 4 compares the values of the original and reconstructed Mueller potential along the TAMD trajectory shown in Fig. 1. As a simple estimate of the error, we used:

$$e_1 = \frac{\int_{\bar{\Omega}} |V(\mathbf{x}) - \tilde{V}(\mathbf{x})| dx}{\int_{\bar{\Omega}} |V(\mathbf{x})| dx} \quad (13)$$

where $\tilde{V}(\mathbf{x})$ denotes the reconstructed potential and $\bar{\Omega}$ is the domain in which the original potential remains less than 180 above its minimum value. The error defined in (13) for this calculation was $e_1 = 4.2 \cdot 10^{-3}$.

These results, which are already very good, can be improved by diminishing d and thereby increasing the number of centers without having to increase the length of the TAMD trajectory. For example, by taking $d = 0.12$, we obtained 351 centers in a trajectory still $2 \cdot 10^4$ steps long. Using these centers to reconstruct the Mueller potential, we obtained $e_1 = 3.2 \cdot 10^{-4}$. The level sets of the reconstructed and original potential defined in Fig. 3 now overlapped so perfectly that they could not be distinguished on the scale of Fig. 3 (data not shown). The optimal σ for this calculation was $\sigma^* = 0.362$, at which value the residual was $e_2(\sigma^*) = 4.7 \cdot 10^{-3}$ and the condition number was $7 \cdot 10^{11}$.

Finally, we note that the result can also be improved by keeping the same distance $d = 0.12$ between centers but increasing the length of the TAMD trajectory. For instance, increasing the number of steps to $5 \cdot 10^4$ produced a reconstruction with an error $e_1 = 7.1 \cdot 10^{-5}$ (data not shown).

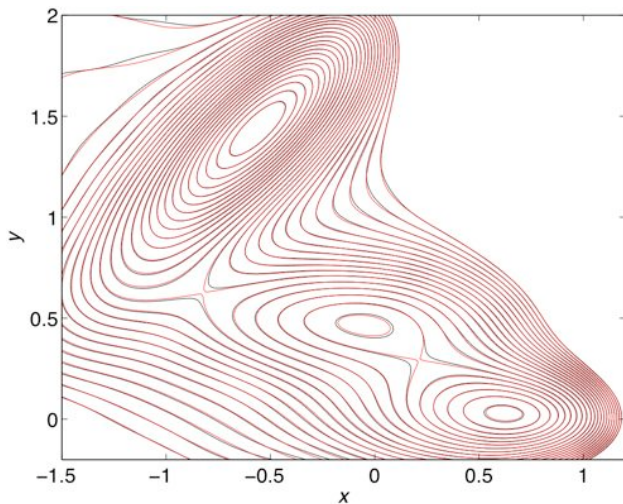


FIG. 3: Comparison between the level sets of the original Mueller potential (red curves) and the reconstructed potential using (2) (black curve). Here we use the 174 centers shown in Fig. 1. The optimal σ is $\sigma^* = 0.398$, see Fig. 2. We show 29 level sets evenly distributed between $V = 0$ and $V = 180$. The level sets of the reconstructed potential and the original one are in so close agreement that they can only be distinguished in some localized regions (e.g. near the saddle point between the two minima in the lower right corner).

IV. COMPARISON WITH METADYNAMICS

Because metadynamics [7, 8] also uses an extended dynamical system for \mathbf{x} and \mathbf{z} and the Gaussian packet (3) to represent $A(\mathbf{z})$, the single-sweep method bears similarities with it. Yet, there is an essential difference between the two methods. Unlike the single-sweep method, metadynamics does not use the mean force, and estimates $A(\mathbf{z})$ by direct sampling, which turns out to be a less efficient way to proceed. Let us elaborate on this claim.

Recall that metadynamics uses an extended system like (8) but where the equation for \mathbf{z} is replaced by [23]

$$\begin{aligned} \gamma \dot{\mathbf{z}} &= \kappa(\boldsymbol{\theta}(\mathbf{x}) - \mathbf{z}) + \sqrt{2\gamma\beta^{-1}} \boldsymbol{\eta}(t) \\ &+ \nu \int_0^t \nabla_{\mathbf{z}} \varphi_{\sigma}(|\mathbf{z}(t) - \mathbf{z}(t')|) dt'. \end{aligned} \quad (14)$$

Here $1/\beta$ is now the physical temperature of the system, and κ and γ are parameters playing the same role as in (8). The integral term in (14) is a flooding term (with $\nu > 0$ controlling the flooding rate) which deposits Gaussian packets $\varphi_{\sigma}(u)$ on the energy landscape wherever $\mathbf{z}(t)$ goes, thereby progressively leveling the effective free energy landscape felt by $\mathbf{z}(t)$. The negative of the integral of the Gaussian packets deposited then gives an approximation of the free energy. For a trajectory with N_{\max} time-steps of size Δt , the time-discretized approximation of this integral reads (compare (2))

$$\tilde{A}(\mathbf{z}) = \nu \Delta t \sum_{n=1}^{N_{\max}} \varphi_{\sigma}(|\mathbf{z} - \mathbf{z}(n\Delta t)|) + C \quad (15)$$

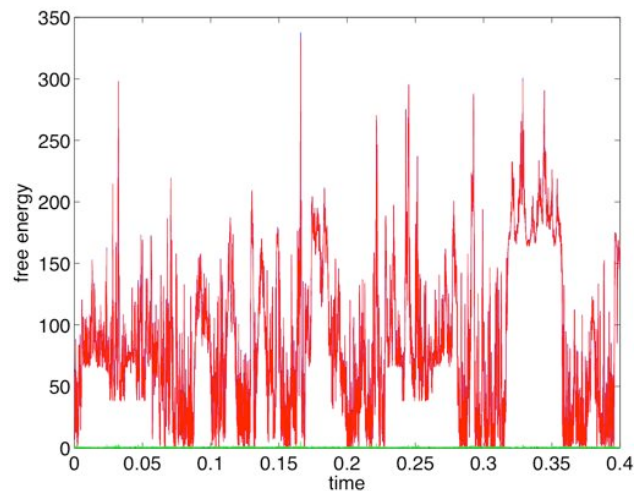


FIG. 4: Comparison between the original (blue line) and reconstructed Mueller potential (red line) computed along the $2 \cdot 10^4$ steps single-sweep trajectory shown in Fig. 1. The green line shows the absolute value of the difference between the two.

where C is a constant used to adjust the height of $\tilde{A}(\mathbf{z})$.

Despite the fact that (15) uses Gaussian packets which are radial-basis functions, the representation (15) is very different from the standard radial-basis representation (2) used in the single-sweep method. In particular, there are no coefficients a_k to adjust in (15). This has the important consequence that, instead of requiring a single sweep across \mathbf{z} -space to get an accurate estimate of the free energy, metadynamics requires that the trajectory revisits many times the same locations in \mathbf{z} -space to deposit centers (i.e. N_{\max} in (15) must be much larger than K in (2) to achieve the same accuracy). This is because the leveling out achieved by the integral term in (14) and, hence, the convergence of the representation (15), only occur statistically [24, 25] (in contrast, the mean force data used at each center in the single sweep method contains already all the statistical information needed at that center). This is consistent with metadynamics being in essence an histogram method, albeit one where the histogram windows are adjusted on-the-fly.

What this entails in terms of efficiency can be illustrated on the two-dimensional Mueller example considered before. In this example, to generate the metadynamics trajectory we used (12) with flooding terms added as in (14), consistent with what was done in Ref. [25] to test the efficiency of metadynamics in a similar set-up. Fig. 5 shows the metadynamics trajectory obtained by integrating (14) for $2 \cdot 10^4$ timesteps with a time-step of $\Delta t = 2 \cdot 10^{-5}$ (same as in the single-sweep method for the results shown in Figs. 1 to 2). As can be seen in Fig. 5, this number of timesteps was enough for the trajectory to visit the important regions of the potential. The reconstructed free energy from this calculation is compared in Fig. 6 to the original one. The metadynamics result is also compared in Fig. 7 to the one obtained

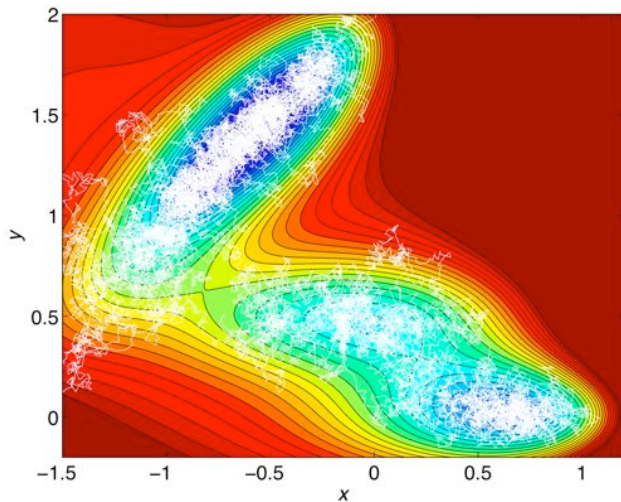


FIG. 5: Metadynamics trajectory (white line) with $2 \cdot 10^4$ steps overlaid on the original Mueller potential.

by the single-sweep method with 174 centers. The error (13) for this metadynamics calculation was $e_1 = 0.16$, i.e. almost two orders of magnitude higher than with the single-sweep method. Fig. 8 shows the original and reconstructed Mueller potential along the metadynamics trajectory (blue and red lines, respectively), together with the absolute value of their difference (green line). By comparing Figs. 4 and 8, it can be seen that the discrepancy between the original and reconstructed potential is much larger with metadynamics than with the single-sweep method on trajectories of the same length. Note that these results clearly indicate that it is not sufficient that the metadynamics trajectory visits once a region on phase space to get an accurate representation of the free energy in this region. This was already noted in Refs. [24, 25].

We were able to improve the metadynamics result by extending the simulation to $2 \cdot 10^5$ steps. The covering of the important regions in the potential was now extensive (data not shown), and the reconstructed potential (data not shown) looked visually better than the one obtained with the shorter trajectory. Yet the error (13) was $e_1 = 0.12$, i.e. still two orders of magnitude larger than the highest error we obtained with the single-sweep method using a 10 times shorter trajectory. We did not attempt to go to longer runs with metadynamics because the memory term in (14) makes such simulations increasingly expensive (their cost scales as the square of the number of timesteps). It should also be stressed that in all these calculations, we optimized the parameters ν , σ and $1/\beta$ the best we could. This optimization, however, turns out to be complicated since there is no systematic way to perform it because, unlike with the single-sweep method, there is no objective function to minimize in metadynamics. The results shown in Figs. 5–8 were obtained with $\nu = 2 \cdot 10^3$, $\sigma = 0.2$ and $1/\beta = 10$.

To be fair, we should conclude this comparison by men-

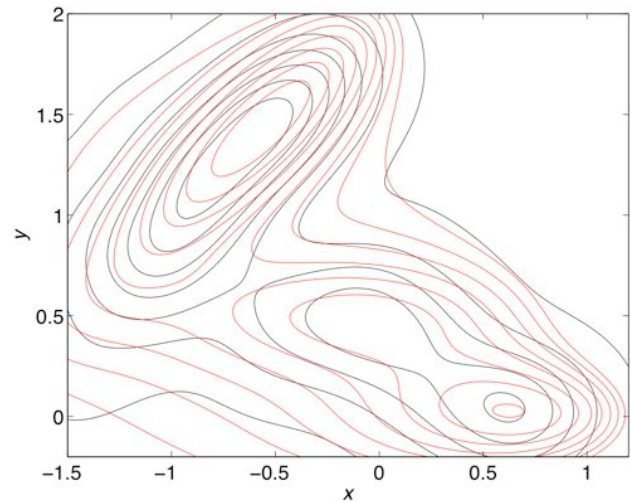


FIG. 6: Comparison between the level sets of the original Mueller potential (red curves) and the reconstructed potential using metadynamics with a trajectory of $2 \cdot 10^4$ steps with a time-step of $\Delta t = 2 \cdot 10^{-5}$ (same as in Figs. 1 and 3). We only use 10 level sets evenly distributed between $V = 0$ and $V = 180$ because the differences between the maps are much bigger than with the single-sweep method and drawing more level sets makes the figure difficult to read. (There are only seven black level sets in the energy reconstructed by metadynamics because it levels off around $V = 140$.)

tioning that the simplicity of the Mueller potential example tends to exaggerate the gain that the single sweep method provides over metadynamics. Indeed, in realistic situations, the single-sweep method also requires to compute the mean force via (11), an operation which was unnecessary in the Mueller example since the force was readily available. Computing the mean force adds an extra cost to the method. It is worth stressing again, however, that the computation of the time averages in (11) can be distributed over several processors. This means that in the ideal situation where the user has at least one processor per center, the effective time to compute all of the mean forces is the same as the one for computing a single one of these forces, i.e. we have perfect scalability. Metadynamics can be parallelized per replica as well, as was proposed in Refs. [26, 27, 28], but not as straightforwardly and not with perfect scalability. Indeed, in all of these versions of metadynamics, the simulated replica are never completely independent from each other.

V. FREE ENERGY OF ALANINE DIPEPTIDE IN SOLUTION

In this section, we use the single-sweep method to reconstruct the free energy of the solvated alanine dipeptide (AD) molecule in two and four torsion angles at 300 K. While AD is not an example of biochemical interest *per se*, we study it because it has been extensively used as a benchmark example for free energy calculations

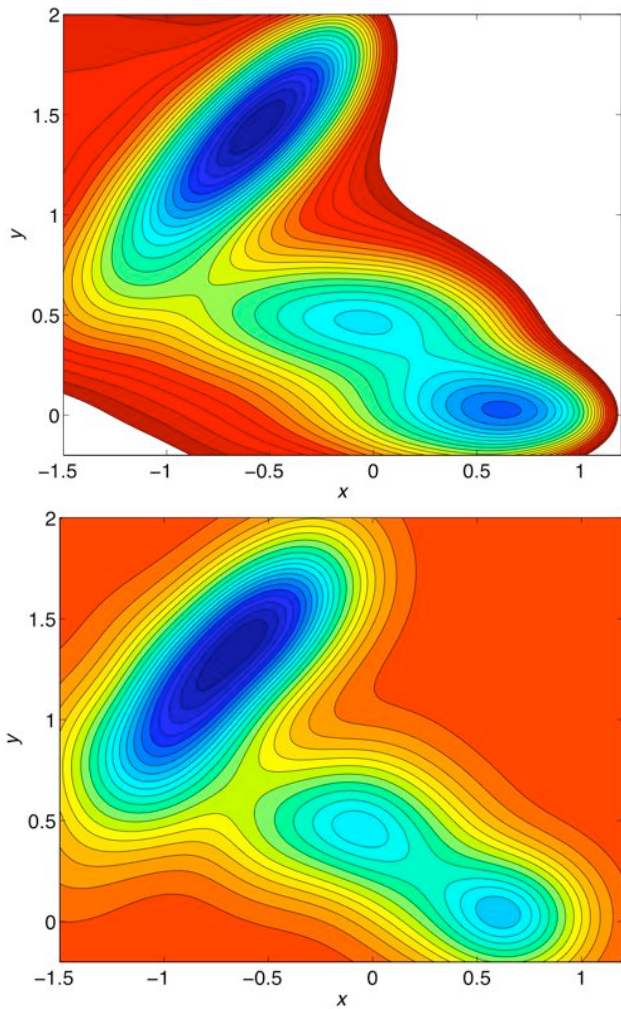


FIG. 7: Comparison between the Mueller potential as reconstructed by the single-sweep method (upper panel) and metadynamics (lower panel) both with a trajectory of $2 \cdot 10^4$ steps and a time-step of $\Delta t = 2 \cdot 10^{-5}$. Other representation of these contourplots were already shown in Figs. 3 and 6 respectively. The map reconstructed by the single-sweep method is very close to the map of the original Mueller potential. The colormaps used in both panels are the same and the reconstructed potentials are shifted so that their minimum is $V = 0$; the white region in the left panel is where the energy is above 180 and is not shown (the result of metadynamics shown in the right panel levels off around $V = 140$ which is why there is no white).

in the literature [6, 29, 30]. On top of this the system is simple enough that we can use it to systematically investigate how the accuracy of the reconstruction method depends on the number of centers and how robust the method is with respect to statistical errors in the input data for the mean forces. Another question we investigate in this section is the robustness of the method against the choice of radial-basis functions. Specifically, we compare results obtained using the Gaussian packet (3) and the

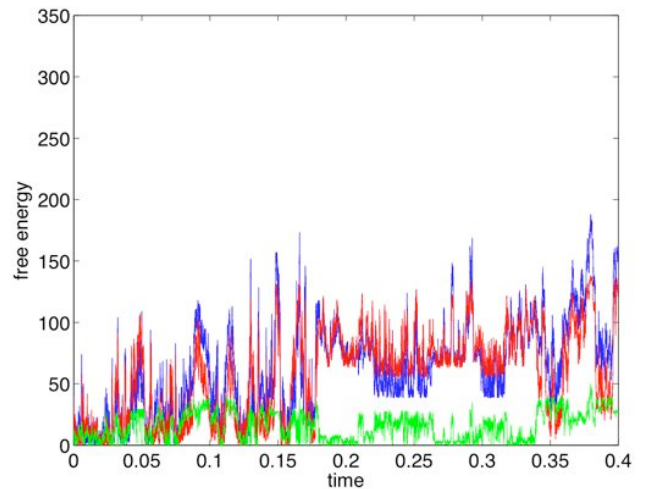


FIG. 8: Comparison of the original (blue line) and reconstructed Mueller potential (red line) computed along the $2 \cdot 10^4$ steps metadynamics shown in Fig. 5. The green line shows the absolute value of the difference between the two. The green line here should be compared with the one in Fig. 4 for the single-sweep method: the discrepancy between the original and reconstructed potential is always larger with metadynamics than with the single-sweep method.

Wendland function

$$\varphi(u) = (1 - u)_+^6 (35u^2 + 18u + 3) \quad (16)$$

where $(f(u))_+ = f(u)$ if $f(u) > 0$, and $(f(u))_+ = 0$ otherwise. (16) is another well-known example of radial-basis function which has the pleasant property that it is compactly supported. This property is appealing in the calculations since it limits the range over which centers interact in (4).

All MD simulations reported below were performed with a version of the MOIL code [31] suitably modified by us, and the AMBER/OPLS [32] force field (for details of the MD set-up see Appendix A).

A. Two angles calculation

We use the standard dihedral angles ϕ and ψ . At 300 K, the system is confined in a region of the (ϕ, ψ) space with $\phi < -50^\circ$ by energy barriers higher than $1/\beta$. In order to overcome these barriers and sweep through the whole $[-180^\circ, 180^\circ]^2$ space, we generated a trajectory by using (8) with $(z_1, z_2) = (\phi, \psi)$, $\kappa = 100$ kcal/mol/rad², a friction coefficient $\gamma = 0.5$ kcal \times ps/mol/rad² and an artificial temperature $1/\bar{\beta} = 9.5$ kcal/mol. With this choice of the parameters, the important regions of the $[-180^\circ, 180^\circ]^2$ space were visited in $4 \cdot 10^4$ steps (40 ps in the time units of the MD variables). The time series of ϕ and ψ along this trajectory are shown in Fig. 9. Variations in κ , γ and $1/\bar{\beta}$ led to qualitatively similar TAMD trajectories, indicating that the the method is robust with regard to

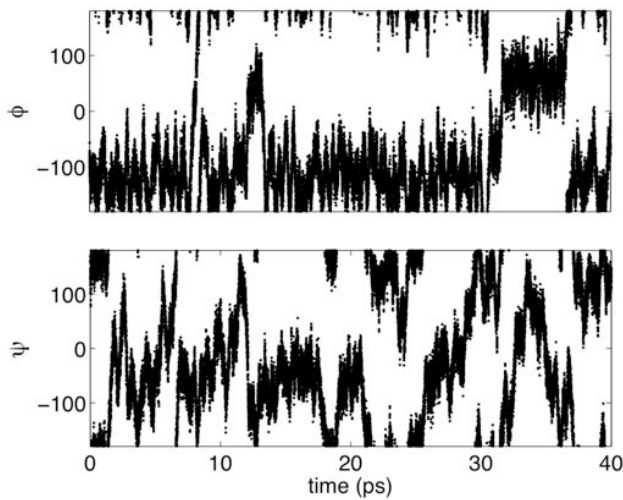


FIG. 9: Time series of the dihedral angles ϕ and ψ along the 40 ps long TAMD trajectory for the solvated alanine dipeptide (AD).

the choice of these parameters. Sets with a different number K of centers were deposited along the TAMD trajectory afterwards by processing this trajectory using various distances d between the centers. Specifically, we generated sets of 90, 128, 151, 188, 219 and 262 centers using, respectively, $d = 31.77^\circ$, 26.00° , 23.87° , 21.37° , 20.00° , 17.92° .

Given a set of K centers (ϕ_k, ψ_k) , we computed the mean forces via K independent MD simulations with restraints at $(\phi, \psi) = (\phi_k, \psi_k)$, i.e. by simulating (10) in the isokinetic ensemble at 300 K, and estimated the mean force via (11) with $\bar{\kappa} = 100$ kcal/mol/rad². This value of $\bar{\kappa}$ was high enough since we checked that the reconstructed free energy remained invariant with higher values of $\bar{\kappa}$ (we did so up to $\bar{\kappa} = 10^3$ kcal/mol/rad²). We then used this data in the reconstruction procedure explained in Sec. II A. Note that since the free energy in the (ϕ, ψ) angle is periodic, we have to periodically extend the centers for the representation. This amounts to changing the representation in (2) into

$$\tilde{A}(\mathbf{z}) = \sum_{\hat{\mathbf{n}} \in \mathbb{Z}^N} \sum_{k=1}^K a_k \varphi_\sigma(|\mathbf{z} - \mathbf{z}_k + 2\pi \hat{\mathbf{n}} \cdot \hat{\mathbf{e}}|) + C, \quad (17)$$

where $\hat{\mathbf{e}}$ is the unit vector in \mathbb{R}^N . In practice, only few periodic replica of the centers are needed (i.e. $\hat{n}_i = 2$ for $i = 1, \dots, N$) because the radial-basis functions centered at the centers further away from the cell under consideration make negligible contributions to the result in this cell.

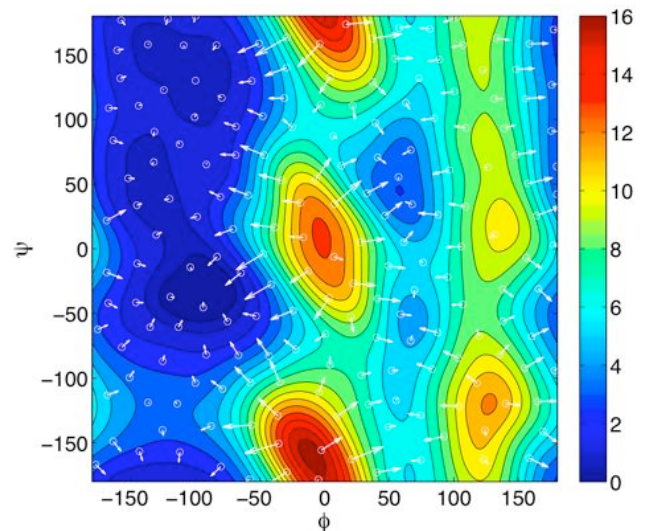


FIG. 10: Free energy of AD in the ϕ and ψ dihedral angles at 300 K calculated with the single-sweep method by using 188 centers deposited at a distance of $d = 21.37^\circ$ from each other. Units for the free energy are kcal/mol, and contour levels are plotted at 0.5 kcal/mol, 1 kcal/mol, and then every 1 kcal/mol. The optimal σ in this reconstruction was $\sigma = 44.73^\circ$. The centers are represented as white circles. At every center, the corresponding mean force vector is also shown. Mean forces were calculated by using (11) with $\bar{\kappa} = 100$ kcal/mol/rad² and $T = 50$ ps.

1. *Calculation with $d = 21.37^\circ$ (188 centers) and $T = 50$ ps.*

We first detail our result with this choice of parameters to pick an example which led to a good balance between accuracy and efficiency. Other choices of parameters are discussed below. Thus, Fig. 10 shows the reconstructed free energy map obtained with $d = 21.37^\circ$ (188 centers) and by computing the mean forces from (11) with $T = 50$ ps. The optimal σ in this calculation was $\sigma^* = 44.73^\circ$. In the figure, the minimum of the free energy is set at 0 kcal/mol, and contour levels are plotted at 0.5 kcal/mol, 1 kcal/mol and then every 1 kcal/mol. The centers are represented as white circles, and the mean forces at the centers as arrows.

Since the free energy map depends on the force field used, comparison with results in the literature is difficult. To assess the accuracy of our result self-consistently, we compared it with the free energy calculated by computing the PDF of ϕ and ψ from a direct MD simulation (DMDS) of about 30 ns. While this trajectory does not cover all the $[-180^\circ, 180^\circ]^2$ space, it covers the important regions and allows for an unbiased estimation of the free energy in these regions which can be used as benchmark. The left panel in Fig. 11 shows the contour levels of the free energy from the single-sweep (black lines) and that from DMDS (red lines). The contour levels are plotted at 0.1 kcal/mol (dotted lines), every 0.5 kcal/mol from

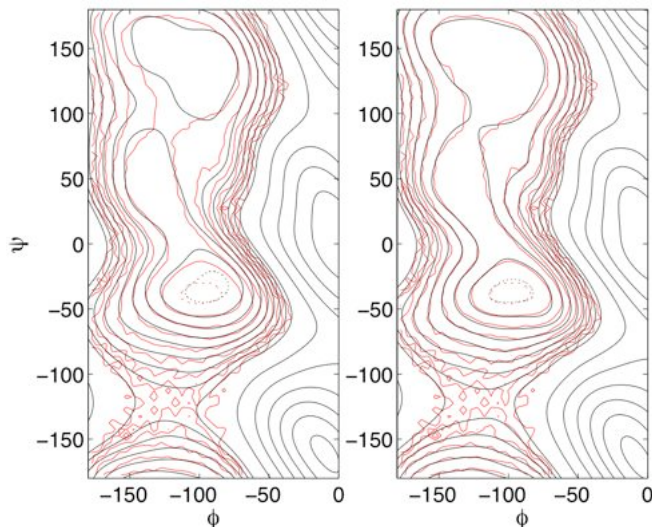


FIG. 11: Comparison between the free energy obtained by single-sweep (black lines) method and DMDS (red lines) for AD. The left panel shows the result with 188 centers, the right panel the one with 262 centers. The contour levels of the free energy are plotted at 0.1 kcal/mol (dotted lines), from 0.5 to 4.0 kcal/mol separated by 0.5 kcal/mol, and then separated by 2 kcal/mol.

0.5 to 4 kcal/mol, and then every 2 kcal/mol. As can be seen, single-sweep results agree remarkably well with those of the DMDS.

In terms of cost, to generate the result shown in Fig. 10, we had to make one simulation run of 40 ps to generate the TAMM trajectory, plus 188 independent runs of 50 ps distributed on different nodes (the additional cost of estimating the parameters a_k^* and σ^* to use in (2) is insignificant). This makes for a total of 9.4 ns of absolute simulation time. However, after distribution, the effective simulation time needed is only 90 ps. On top of this, we show below that a good estimate of the free energy can be obtained with as low as 90 centers (i.e. with an absolute simulation time of 4.5 ns and the same effective simulation time, 90 ps). For comparison, in Ref. [30] Ensing *et al.* report a 4 ns calculation performed with metadynamics to estimate the free energy of AD in ϕ and ψ . It is not clear how well this metadynamics calculation can be parallelized to reduce its effective cost (it was not parallelized in Ref. [30]). In addition, the result of this metadynamics calculation is unlikely to be as accurate as the one in Fig. 10 (in Ref. [30] no comparison like the one shown in Fig. 11 is provided)

2. Robustness and convergence analysis

Next we analyze how robust are the results with respect to the statistical error in the mean force data and the choice of radial-basis function. We also analyze convergence in function of the number of centers. As ref-

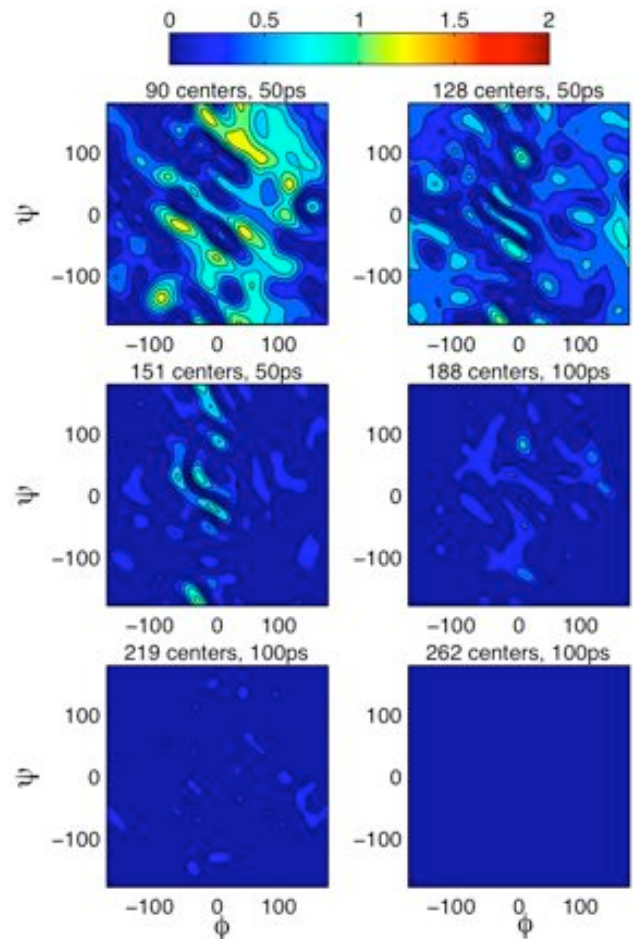


FIG. 12: Difference maps with respect to the AD free energy in ϕ and ψ reconstructed with Gaussian functions using 262 centers and $T = 250$ ps. The figures in the different panels correspond to various number of centers and length of time averaging for the mean forces, as indicated. Units are kcal/mol. Note that the scale of the colormap is different from the one in Fig. 10. In particular, the differences are mostly below 0.5 kcal/mol with 151 centers and 50 ps simulations already.

erence value, we take the free energy reconstructed with $d = 17.92^\circ$ (262 centers) and $T = 250$ ps of time averaging in (11). The map of the free energy calculated with these parameters (data not shown) is visually very similar to the one shown in Fig. 10, but it is more accurate. The residual error can be estimated from the right panel of Fig. 11 which shows the contour levels of the free energy from the single-sweep (black lines) and that from DMDS (red lines): these level sets coincide up to statistical errors in the DMDS, indicating that the free energy provided by the single sweep method with 262 centers and $T = 250$ ps can indeed be taken as an “exact” benchmark.

Fig. 12 shows the differences between the map of the reference free energy reconstructed with $d = 17.92^\circ$ (262 centers) and $T = 250$ ps and those reconstructed with less centers and shorter restrained simulations. The largest

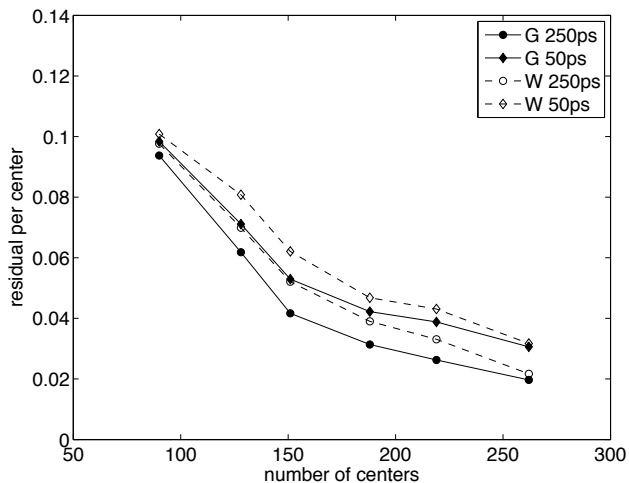


FIG. 13: Residual per center versus number of centers in the reconstruction of the AD free energy in ϕ and ψ angles. Data are from calculations with different time averaging length, using Gaussian (G) and Wendland (W) basis functions.

errors are in the regions corresponding to the highest peaks of the free energy (these are also the regions where the least centers were deposited). The differences never exceed 1.25 kcal/mol with 90 centers and $T = 50$ ps and they fall mostly below 0.5 kcal/mol with 151 centers and $T = 50$ ps already.

We also compared the quality of the reconstruction of the free energy when using Gaussian (3) and Wendland (16) basis functions. Fig. 13 shows the residual per center versus the number of centers for AD, by using Gaussian (filled symbols) and Wendland (empty symbols) basis functions, using $T = 50$ ps (diamonds) and $T = 250$ ps (circles) long restrained simulations to estimate the mean forces. At equal values of K and T , the reconstruction is slightly more accurate with Gaussian than with Wendland functions, though these differences turn out to be quite small in terms of the free energy maps themselves (data not shown).

Using longer simulations for the mean force (which means a smaller random error on these forces) also improves the results. With 262 centers and $T = 250$ ps long simulations for the mean forces, the maps reconstructed with Gaussian and Wendland basis functions were almost identical (data not shown), and they were not significantly different from the map shown in Fig. 10. These results, however, were obtained at very different values of optimal σ : $\sigma^* = 26.33^\circ$ with Gaussians and $\sigma^* = 123.20^\circ$ with Wendland functions. The condition numbers at the optimal σ were 3889.67 and 868.86, respectively, which is low. Note that the same trends here described were observed in a periodic test case for which the potential was known exactly (data not shown).

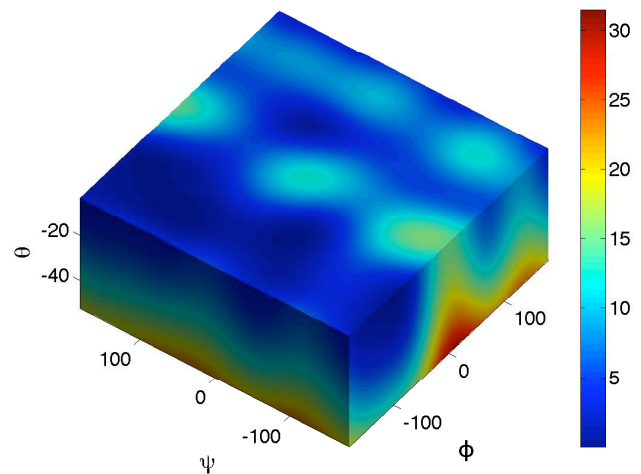


FIG. 14: Free energy of AD in the ϕ , ψ , θ angles obtained from the marginal in these angles of the PDF associated with the free energy in four angles $\tilde{A}(\phi, \psi, \theta, \zeta)$. Data are represented for $\theta \in [-50^\circ, -3^\circ]$. Note that the scale of the colormap is different from the one in Fig. 10

B. Four angles calculation

As a second more challenging test, we computed the free energy of AD in the four torsion angles, ϕ , ψ , θ , and ζ . A TAMD trajectory of 44 ps was generated by using (8) with $(z_1, z_2, z_3, z_4) = (\phi, \psi, \theta, \zeta)$, $\kappa = 100$ kcal/mol/rad², an artificial temperature $1/\bar{\beta} = 9.5$ kcal/mol, friction coefficients $\gamma = 0.5$ kcal \times ps/mol/rad² for ϕ and ψ and $\gamma = 1$ kcal \times ps/mol/rad² for θ and ζ . The MD potential keeps the amide planes in *trans* configuration, and so θ and ζ were varying in the range $[-70^\circ, 70^\circ]$. In 44 ps, the TAMD trajectory covered well the accessible state space for ϕ , ψ , θ and ζ , in the sense that the time series for these angles were similar in their respective state space to those shown in Fig. 9 (notice however that extensive coverage of the four-dimensional space is unlikely in so short a run). Along the TAMD trajectory, 200 centers at a distance of $d = 45.84^\circ$ were deposited. At these centers, the mean forces \mathbf{f}_k were computed by using (11) with $\bar{\kappa} = 100$ kcal/mol/rad² and $T = 50$ ps (i.e. the absolute time of simulation was about 10 ns, but the effective time after distribution was 94 ps only). We used these \mathbf{f}_k in the objective function (4) to finally get the representation (2) of the four-dimensional free energy $\tilde{A}(\phi, \psi, \theta, \zeta)$. The optimal σ in this representation was $\sigma^* = 67.63^\circ$ and the condition number at this value of σ was 4214.05.

Since a full graphical representation of $\tilde{A}(\phi, \psi, \theta, \zeta)$ is not possible, we did several tests to validate our result. Fig. 14 shows the three dimensional free energy $\tilde{A}(\phi, \psi, \theta)$ obtained from the marginal in these angles of the PDF associated with $\tilde{A}(\phi, \psi, \theta, \zeta)$. This marginal was calculated *a posteriori* by numerical integration over ζ of $e^{-\beta\tilde{A}(\phi, \psi, \theta, \zeta)}$ with the full $\tilde{A}(\phi, \psi, \theta, \zeta)$ reconstructed by the single-sweep method. The map is reasonable, and

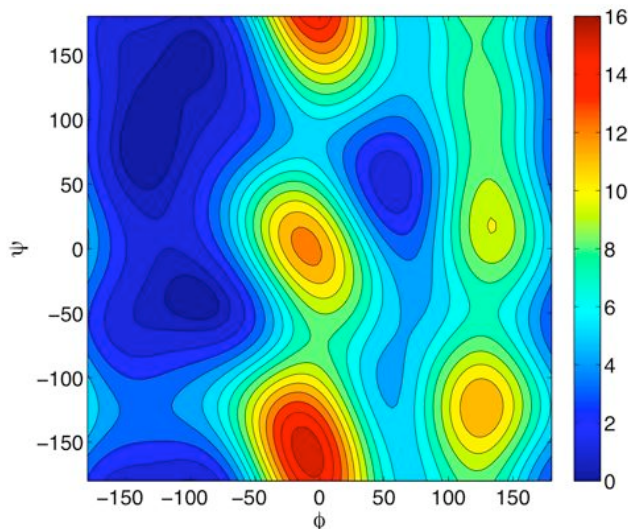


FIG. 15: Free energy of AD in the ϕ , ψ angles obtained from the marginal in these angles of the probability density associated with the free energy in four angles $\tilde{A}(\phi, \psi, \theta, \zeta)$. Contour levels are as in Fig. 10. Note the remarkable agreement between this map and the one shown in Fig. 10.

shows nontrivial features in all three directions. Fig. 15 shows the two dimensional free energy $\tilde{A}(\phi, \psi)$ obtained from the marginal in these angles of the PDF associated with $\tilde{A}(\phi, \psi, \theta, \zeta)$. The map is in remarkably good agreement with the one in Fig. 10.

As a further test of accuracy, we re-calculated the mean force using (10) and (11) using a different set of centers than those used in (2). Then we estimated the relative error between these mean forces and the ones obtained by taking the negative gradient of the reconstructed $\tilde{A}(\phi, \psi, \theta, \zeta)$ using the original set of centers and mean forces:

$$\varepsilon_k = \frac{|\nabla_z \tilde{A}(\mathbf{z}_k^n) + \mathbf{f}_k^n|}{|\mathbf{f}_k^n|} \quad (18)$$

where \mathbf{z}_k^n are the new centers and \mathbf{f}_k^n are the mean forces at these centers. The new centers were 20 points chosen at random in the domains $\phi, \psi \in [-180^\circ, 180^\circ]$, $\theta, \zeta \in [-70^\circ, 70^\circ]$.

Fig. 16, top panel, shows, for each of these centers, the distance from the closest of the 200 centers (black line). Data are compared to the minimal distance between the 200 centers (red dashed line). This result shows that, with $d = 45.84^\circ$, these centers fill properly the four dimensional domain in the sense that every new center is always a distance about d to one of the original centers. Fig. 16, middle panel, shows the relative error ε_k for $k = 1, \dots, 20$ (black solid line), when $T = 50$ ps long restrained simulations are used to compute the mean forces. The mean value of ε_k (black dashed line) is 0.14, with standard deviation 0.09 and maximum value 0.47. For comparison, the mean value of the relative residual per center (red dashed line) is 0.09, with standard deviation 0.06 and maximum value 0.39

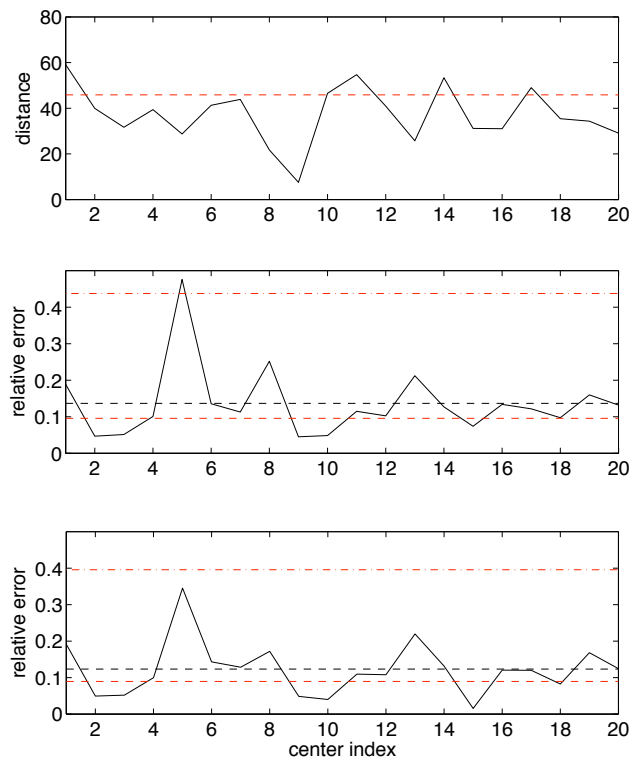


FIG. 16: Accuracy of the reconstruction of the free energy of AD in four angles. Top panel, distance of each of the random centers from the closest of the 200 centers (black line), compared with the minimal distance between the 200 centers (red line). Middle and lower panel, relative error ε_k defined in (18) for mean forces computed respectively from 50 and 250 ps restrained simulations: the error ε_k (black solid line) and its mean value (black dashed line), compared with the mean value of the relative residual per center for the 200 centers set (red dashed line) and its maximum value (red dashed-dotted line).

ation 0.06 and maximum value 0.44 (red dashed-dotted line). Fig. 16, bottom panel, shows ε_k when $T = 250$ ps long restrained simulations are used to compute the mean forces. In this case, the mean value of ε_k (black dashed line) is 0.12, with standard deviation 0.07 and its maximum value is 0.34. For comparison, the mean value of the relative residual per center (red dashed line) is 0.09, with standard deviation 0.06 and maximum value 0.39 (red dashed-dotted line).

These results show that, in points away from the original centers, the reconstructed free energy is as accurate as it is at the centers, which is clearly the best we can hope for.

VI. CONCLUDING REMARKS

In summary, we have proposed a method for the calculation of free energies which is simple, accurate, and efficient. Unlike standard histogram methods such as

WHAM and metadynamics, the single-sweep method uses the mean force computed at a set of centers to reconstruct the free energy. This set of centers is determined using TAMD to rapidly sweep through the important regions of the free energy, and the mean forces at these centers are estimated in a standard way via the computation of a conditional expectation using time-averaging along restrained or constrained simulations. From these data, the free energy $A(\mathbf{z})$ is then reconstructed globally by minimization of an objective function to determine the coefficients in a radial-basis function representation of $A(\mathbf{z})$. If convenient, this reconstruction step can use data for the centers and the mean forces obtained by other means than TAMD.

Compared with histogram methods and metadynamics, the single-sweep technique combines several advantages:

- It does not require *a priori* knowledge of the free energy since it uses TAMD to find the important regions in the landscape automatically.
- The most costly step of the calculation, namely the computation of the mean forces at the centers, can be straightforwardly distributed on different, independent, processors.
- The reconstruction step is variational, i.e. the optimal coefficients in the free energy representation are determined automatically, which limits the number of parameters to adjust beforehand.
- The results can be easily monitored for convergence, and systematically improved if desired. In particular, new centers can be added on top of previous ones along the same TAMD trajectory to increase the accuracy without having to repeat the previous calculation.
- The method can be used in more than 2 dimensions and its computational complexity is the same regardless of the dimension.

We believe that these features make the single-sweep method appealing to calculate the free energy of systems more complicated but also more interesting than the ones studied in this paper.

Acknowledgments

We thank Giovanni Ciccotti and David Chandler for carefully reading the manuscript; Weinan E for pointing out sparse grid methods which prompted us to test our method in four dimensions; Ron Elber and Anthony West for their help with the MOIL code; Sara Bonella, Simone

Meloni, Michele Monteferrante and Maddalena Venturoli for useful discussions; and finally, Eric Darve for suggesting the test using (18). This work was partially supported by NSF grants DMS02-09959 and DMS02-39625, and by ONR grant N00014-04-1-0565.

APPENDIX A: DETAILS OF THE MD SIMULATIONS

All MD simulations were performed with the MOIL code [31], and the AMBER/OPLS [32] force field as implemented in the code. A starting structure for the AD molecule ($\text{CH}_3\text{-CO-NH-C}_\alpha\text{HCH}_3\text{-CO-NH-CH}_3$) was solvated in a box of 252 water molecules of volume $(20 \text{ \AA})^3$. Periodic boundary conditions were used. Van der Waals interactions were truncated at 9 Å. Electrostatic interactions were treated with the Particle Mesh Ewald method [33] with real space cutoff 9 Å, a grid of 32^3 points, and 4-th order *B*-splines for the interpolation of the structure factor (in order to be in the high accuracy range [33]). The TIP3 model [34] was used for the water molecules. Non-bonded interaction lists were updated every 10 steps. All chemical bonds in the system were kept fixed with the SHAKE algorithm [35]. Amide planes were restrained to be always in *trans* configuration. The Velocity Verlet algorithm was used for the dynamics of the Cartesian variables with time-step 1 fs, and all velocities were scaled at every step to keep the temperature at 300 K. In order to obtain the initial configuration for the temperature accelerated MD simulation (TAMD), the system was first equilibrated for 100 ps by keeping the solute molecule fixed (i.e. by zeroing forces and velocities of its atoms) and by assigning to all water atoms at every step velocities sampled from a Maxwell distribution at 300 K. Then, the whole system was simulated for 400 ps for equilibration. The torsion angles used in the simulations are defined by the quadruplets of atoms (C,N,C $_\alpha$,C) and (N,C $_\alpha$,C,N) for ϕ and ψ , and (O,C,N,C $_\alpha$) and (C $_\alpha$,C,N,H) for θ and ζ . In the TAMD simulation, the equations of motion of the collective variables were integrated with the forward Euler scheme with time-step 1 fs, $\gamma = 0.5 \text{ kcal}\times\text{ps}/\text{mol}/\text{rad}^2$ for ϕ and ψ and $\gamma = 1 \text{ kcal}\times\text{ps}/\text{mol}/\text{rad}^2$ for θ and ζ . The force constant for the restraint potential was $\kappa = 100 \text{ kcal}/\text{mol}/\text{rad}^2$, and the effective temperature such that $\bar{\beta}^{-1} = 9.5 \text{ kcal}/\text{mol}$. The Cartesian coordinates of water and AD atoms were saved during the TAMD simulation. In this way, for every center \mathbf{z}_k deposited along the trajectory in collective variables space, there is a corresponding configuration \mathbf{x}_k of the system in Cartesian space such that $\theta(\mathbf{x}_k) \approx \mathbf{z}_k$. We used these configurations as initial conditions for the restrained simulations at the centers. Data for the mean force calculations were accumulated after further relaxation of the system for 5 ps.

[1] E. M. Boczeko and C. L. Brooks 3rd, Science. **269**, 393 (1995).

[2] T. Simonson, G. Archontis, and M. Karplus, Acc. Chem.

- Res. **35**, 430 (2002).
- [3] J. D. Faraldo-Gómez and B. Roux, Proc. Natl. Acad. Sci. U.S.A. **104**, 13643 (2007).
- [4] S. Kumar, J. M. Rosenberg, D. Bouzida, R. H. Swendsen, and P.A. Kollman, J. Comput. Chem. **13**, 1011 (1992).
- [5] G. M. Torrie and J. P. Valleau, Chem. Phys. Lett. **28**, 578 (1974).
- [6] C. Bartels and M. Karplus, J. Comput. Chem. **18**, 1450 (1997).
- [7] A. Laio and M. Parrinello, Proc. Natl. Acad. Sci. U.S.A. **99**, 12562 (2002).
- [8] A. Iannuzzi, A. Laio, and M. Parrinello, Phys. Rev. Lett. **90**, 238302 (2003).
- [9] E. A. Carter, G. Ciccotti, J. T. Hynes, and R. Kapral, Chem. Phys. Lett. **156**, 472 (1989).
- [10] J. G. Kirkwood, J. Chem. Phys. **3**, 300 (1935).
- [11] L. Maragliano and E. Vanden-Eijnden, Chem. Phys. Lett. **426**, 168 (2006).
- [12] J. VandeVondele and U. Rothlisberger, J. Phys. Chem. B. **106**, 203 (2002).
- [13] L. Rosso, P. Mináry, Z. Zhu, and M. E. Tuckerman, J. Chem. Phys. **116**, 4389 (2002).
- [14] I. Foster and C. Kesselman, *The Grid 2: Blueprint for a New Computing Infrastructure*. (Morgan Kaufmann, 2003).
- [15] F. Berman, G. Fox, A. J. G. Hey (Eds.), *Grid Computing: Making The Global Infrastructure a Reality*. (John Wiley & Sons, 2003)
- [16] R. Schaback, Adv. Comp. Math. **3**, 251 (1995).
- [17] M. D. Buhmann, Acta. Numer. **9**, 1 (2000).
- [18] P. Niyogi and F. Girosi, Adv. Comp. Math. **10**, 51 (1999).
- [19] H.-J. Bungartz H-J and M. Griebel, Acta. Numer. **13**, 1 (2004).
- [20] G. Ciccotti, R. Kapral, and E. Vanden-Eijnden, Chem. Phys. Chem. **6**, 1809 (2005).
- [21] G. Ciccotti, T. Lelièvre, and E. Vanden-Eijnden, Comm. Pure. App. Math. to appear (available from “early view”).
- [22] K. Mueller, Angew. Chem. **19**, 1 (1980).
- [23] A term $m_z \ddot{z}$ is typically added to (14) and the thermostat can be different, but this is not essential for our discussion and does not change our conclusions.
- [24] T. Lelièvre, M. Rousset, G. Stoltz, J. Chem. Phys. **126**, 134111 (2007).
- [25] G. Bussi, A. Laio, and M. Parrinello, Phys. Rev. Lett. **96**, 090601 (2006).
- [26] P. Raiteri, A. Laio, F. L. Gervasio, C. Micheletti, and M. Parrinello, M. J. Phys. Chem. B. **110**, 3533 (2005).
- [27] G. Bussi, F. L. Gervasio, A. Laio, and M. Parrinello, J. Am. Chem. Soc. **128**, 13435 (2006).
- [28] S. Piana and A. Laio, J. Phys. Chem. B. **111**, 4553 (2007).
- [29] L. Rosso, J. B. Abrams, and M. E. Tuckerman, J. Phys. Chem. B, **109**, 4162 (2005).
- [30] B. Ensing, M. De Vivo, Z. Liu, P. Moore, and M. L. Klein, Acc. Chem. Res. **39**, 73 (2006).
- [31] R. Elber, A. Roitberg, C. Simmerling, R. Goldstein, H. Li, G. Verkhivker, C. Keasar, J. Zhang, and A. Ulitsky, Comp. Phys. Comm. **91**, 159 (1995).
- [32] W. L. Jorgensen and J. Tirado-Rives, J. Am. Chem. Soc. **110**, 1657 (1998).
- [33] U. Essmann, L. Perera, M. L. Berkowitz, T. Darden, H. Lee, and L. G. Pedersen, J. Chem. Phys. **103**, 8577 (1995).
- [34] W. L. Jorgensen, J. Chandrasekhar, J. D. Madura, R. W. Impey, and M. L. Klein, J. Chem. Phys. **79**, 926 (1983).
- [35] J. P. Ryckaert, G. Ciccotti, H. J. C. Berendsen, J. Comput. Phys. **23**, 327 (1977).